

# Image Segmentation of Thermal Waving Inspection based on Particle Swarm Optimization Fuzzy Clustering Algorithm

Jin Guofeng<sup>1</sup>, Zhang Wei<sup>1</sup>, Yang Zhengwei<sup>1</sup>, Huang Zhiyong<sup>1</sup>,  
Song Yuanjia<sup>2</sup>, Wang Dongdong<sup>1</sup>, Tian Gan<sup>1</sup>

1. 602 office, Xi'an Research Institute of High Technology, Hongqing Town, Xi'an 710025, China, douhao616@126.com  
2. China Aerodynamics Research and Development Center, Mianyang 621000, China

The Fuzzy C-Mean clustering (FCM) algorithm is an effective image segmentation algorithm which combines the clustering of non-supervised and the idea of the blurry aggregate, it is widely applied to image segmentation, but it has many problems, such as great amount of calculation, being sensitive to initial data values and noise in images, and being vulnerable to fall into the shortcoming of local optimization. To conquer the problems of FCM, the algorithm of fuzzy clustering based on Particle Swarm Optimization (PSO) was proposed, this article first uses the PSO algorithm of a powerful global search capability to optimize FCM centers, and then uses this center to partition the images, the speed of the image segmentation was boosted and the segmentation accuracy was improved. The results of the experiments show that the PSO-FCM algorithm can effectively avoid the disadvantage of FCM, boost the speed and get a better image segmentation result.

**Keywords:** Image segmentation, thermal wave inspection, particle swarm optimization, fuzzy C-Mean clustering algorithm

## 1. INTRODUCTION

INFRARED THERMAL WAVE testing method is a non-destructive testing method that has developed rapidly in recent years. The interaction of the various heated excitations and the materials are used for the infrared thermal wave technique method to detect the unevenness or anomaly inside the materials [1]. Compared to X-ray testing, ultrasonic testing and other traditional non-destructive testing methods, the infrared thermal wave testing method has the following advantages: high-speed, non-contact, safe, single-side test, quantitative detection, and others. It has gained great acceptance in wide application areas, e.g., aviation, navigation, power, automotive, construction and other areas [2]-[10].

The image sequences captured by thermal camera contain abundant defect information, which is used for recognizing the defects. However, the testing process is impacted by a variety of factors of images, their narrow dynamic range, low-resolution and high noise. So, the infrared image sequences have to be analyzed quantitatively and qualitatively to calculate defect sizes and depths accurately. Image segmentation is the basic problem of image processing which aims to partition images into meaningful regions and extract the target out of the complex background for the subsequent quantitative identification [11].

Infrared thermal image segmentation is the process that separates regions of deviant temperature from the image. This segmentation can be seen as a clustering process for pixels that have different characteristics, as pixel gradient and their pixel neighborhood characteristics. Clustering is an unsupervised classification method. The overall distribution pattern of data and the interrelationships among data can be found by this approach, so it is a powerful intelligent image segmentation method. FCM is a clustering algorithm that is widely used because of better results and higher efficiency. The disadvantages of FCM are: it can easily be trapped to

local minima and it is sensitive to initial values and noises. If the initial values are not selected suitably, the data may be misclassified. To overcome shortages of the FCM, a fuzzy C-mean clustering algorithm based on the particle swarm optimization (PSO) is proposed in this paper.

## 2. THEORY OF ALGORITHMS

### 2.1. Particle Swarm Optimization Algorithm

Particle swarm optimization (PSO) algorithm proposed by Kennedy and Eberhart in 1995, is a technique of evolution computation. This swarm intelligence is motivated by the search strategy of defense and hunting behavior of birds, fishes and other biological communities. It has been widely used in the function optimization, neural network training, pattern recognition, image processing and other engineering fields. In  $D$ -dimensional space, the evolution equation of the standard PSO algorithm is expressed as:

$$v_{(i+1)d} = \omega v_{id} + c_1 r_1 (p_{id} - x_{id}) + c_2 r_2 (p_{gd} - x_{id}) \quad (1)$$

$$x_{(i+1)d} = x_{id} + v_{id} \quad (2)$$

Here,  $i=1,2,\dots,n$ ;  $d=1,2,\dots,D$ .  $\omega$  is the inertia weight that usually decreases linearly from 0.9 to 0.2. The learning factors  $c_1$  and  $c_2$  are non-negative constants which represent the weight of the particle preferences,  $c_1$  represents the preference of their own experience,  $c_2$  represents the preference of the group experience. According to the experience,  $c_1$  and  $c_2$  are set to 2.05 in practice [12]. The random numbers  $r_1$  and  $r_2$  get the values between (0, 1). The velocity vector  $v_{id} \in [-v_{\max}, v_{\max}]$ ,  $v_{\max}$  is a constant, set according to different problems, a smaller value of  $v_{\max}$  will slow down the convergence rate and efficiency. According to specific issues, the iteration termination condition is

generally chosen as the maximum number of iterations, or it can be set as the particle swarm best position satisfying the minimum threshold scheduled.

## 2.2. Fuzzy C-Mean Clustering Algorithm

Clustering is an unsupervised method of machine learning which does not have any prior understanding about the distribution of the data. It is a process that assort the objects into groups (called clusters), so that the objects in the same clusters are more similar (in some sense or another) to each other than to those in other clusters. FCM was advanced on the hard C-means (HCM) algorithm. Based on the least square principle, the clusters of data field were obtained by applying the iterative method to optimize the objective function.

Basic principle of the FCM that partitions the target data set  $X$  (with  $n$  samples) into classes  $c$  (where  $2 \leq c \leq n$ ) is to find the membership function  $(u_{ij})_{c \times n}$  and the center  $B=(v_1, v_2, \dots, v_c)$  of all  $c$  classes to search for a minimum of the given objective function that is expressed in the form:

$$J = \sum_{i=1}^c \sum_{j=1}^n (u_{ij})^m d^2(x_i, x_j) \quad (3)$$

Here,  $m \in [1, \infty)$  is the weight index, a constant that controls the degree of fuzzy clustering results.  $d(x_i, x_j)$  is the Euclidean distance of the  $j$ -th sample to the  $i$ -th class.

When

$$\sum_{i=1}^c u_{ij} = 1$$

according to the Lagrange multiplier method, the necessary conditions of the objective function taking the minimum are expressed as:

$$u_{ij} = \frac{1}{\sum_{k=1}^c \left[ \frac{d_{ij}}{d_{kj}} \right]^{\frac{2}{m-1}}} \quad (4)$$

$$v_i = \frac{1}{\sum_{j=1}^n (u_{ij})^m} \sum_{k=1}^n (u_{ik})^m x_k \quad (5)$$

If the data set  $X$ , the number of clustering categories  $c$  and the weight index  $m$  are known, the best classification matrix and the cluster centers are expressed by the above two equations.

The efficiency indicator *PBMF* is chosen to evaluate the effect of the clustering results, which is the maximum index of the optimal number of the clusters; the greater its value, the better the clustering results. It is defined as [13]:

$$PBMF(c) = \frac{1}{c} \times \frac{E_1 \max_{i,j} \|v_i - v_j\|}{\sum_{i=1}^c \sum_{j=1}^n u_{ij}^m \|x_j - x_i\|} \quad (6)$$

where  $E_1$  is a constant associated with the data sets;  $m$  is the ambiguity;  $x_j, v_i, u_{ij}$  represent a single sample, the center vector of a cluster and an element of the plotting matrix, respectively.

## 2.3. Principle of the FCM based on PSO

When FCM is applied to image segmentation, the gray histogram of the image is used to substitute the sample data to reduce computation and to increase the speed level [14]-[15]. The objective function of the fast FCM based on the gray histogram is defined as:

$$W_m(U, V) = \sum_{j=0}^L \sum_{i=1}^c (u_{ij})^m (d_{ij})^2 h(j) \quad (7)$$

where  $h(j)$  is the gray level histogram of the obtained image,  $j$  denotes a level of the gray scale,  $j=0 \sim L$ ,  $L$  is the maximum level.  $u_{ij}$  is the membership of the  $j$ -th gray level in the  $i$ -th class,  $d_{ij}$  is the distance of the  $j$ -th gray level to the  $i$ -th class, which is defined by  $(d_{ij})^2 = \|j - z_i\|^2$ ,  $z_i$  is the gray value of the  $i$ -th cluster center.

When the FCM-PSO is applied to image segmentation, each pixel in the image is evaluated by fitness function, defined as:

$$f(x_i) = \frac{\lambda}{W_m(U, V)} \quad (8)$$

Here,  $\lambda$  is a constant,  $W_m(U, V)$  is the sum of the total between-class dispersion number. The smaller the  $W_m(U, V)$ , the better effect of the cluster, the higher individual fitness.

The implemented steps of the algorithm are:

Step 1: Initialize the particle swarm parameters. Given the fuzzy index  $m$ , the population size  $n$ , the learning factors  $c_1$  and  $c_2$ , the inertia weight  $\omega_{\max}$  and  $\omega_{\min}$ , the maximum number of iterations  $I_{\max}$ , the number of the classification categories  $c$ . Then, select the initial cluster center of the  $c$  sample points randomly, calculate the membership matrix composed of a particle from the cluster center, and initialize the particle velocity. Finally,  $n$  particles were produced after  $n$  times computation.

Step 2: Initialize the cluster parameters. Set the number of fuzzy index  $m$ , the initial number of clusters  $c$ , the maximum number of clusters  $c_{\max}$ , and the threshold  $e$ .

Step 3: Calculate the degree of membership and membership matrix. According to the basic steps of the clustering algorithm, calculate the new cluster center and the corresponding membership matrix by (4) and (5). The calculated results form a particle.

Step 4: According to (8) evaluate the sufficiency of the particles, then track and record the extreme value of each individual particle and the global extreme of the particle swarm. Update the position and the velocity of the particle using (1) and (2).

Step 5: Recalculate the degree of membership and membership matrix. For the new particle obtained from the particle swarm, calculate the membership matrix of its corresponding cluster center.

Step 6: Determine whether the iteration termination conditions meet the requirements. If the iterated result is satisfied, calculate the validity of the indicators  $PBMF(c)$  by (6), then finish the algorithm, otherwise return to step 4.

Step 7: If  $c < c_{max}$ , then  $c=c+1$ , go to step 3. Otherwise continue.

Step 8: Identify the maximum value of  $PBMF(c)$ , corresponding to which  $c$  is the optimal number of clusters, and the corresponding  $U$  and  $V$  are the optimal clustering results.

### 3. EXPERIMENTS AND IMAGE CAPTURING

The experiments were performed on the pulsed heating infrared thermal wave non-destructive test system, produced by the Thermal Wave Imaging (TWI), Inc., USA. The testing system is shown in Fig.1. Two linear xenon flash lamps were assembled as the pulsed thermal excitation device, with the maximum power output of each flash being 4.8 KJ. The type of the infrared camera is Thermal CAM™ SC3000, which is produced by the FLIR Company in Sweden, and the working wave band of the thermal camera is 8~9  $\mu\text{m}$ , the temperature sensitivity at room temperature is 0.02 K, the imaging camera for the 40 wide-angle lens, the testing area at a fixed distance of 42 cm is 24 cm  $\times$  32 cm.

The specimens used in the experiment are shown in Fig.2. (a) is a steel shell specimen map containing five different diameter flat-bottomed holes to simulate the debonding defect. (b) is a composite specimen, which is made of two layers of composite materials suppressed, it contains three artificial circular defects of different diameters.

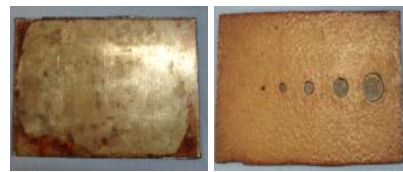
The surfaces of the experimental specimens are painted with black lacquer because it can improve the emissivity and absorptivity of the specimens [16]-[17]. When testing, the frequency of IR camera was set to 60 Hz, the capturing time was set to 30 s.

The original thermal image sequences of test surfaces of the two specimens gained in the experiments are shown in Fig.3 and Fig.4, respectively, which were captured by the camera and recorded by computer. Abundant defect information is contained in thermal images. The areas of the surface temperature anomaly (hot spots) correspond to the defects in the specimen. From Fig.3, it is clearly seen that the defects appear firstly at time 0.43s, the bigger the defect, the bigger the hot spot. Along with the time, the contrast of defects and other area is growing, reaching the maximum at 4.7s. Then the contrast is dropping with the hot spots becoming faint because of the lateral thermal diffusion. At last, the surface temperature distribution becomes balanced and no defect information can be seen in the image. The smallest defect, however, is not visible at all.

Compared with the testing for steel shell, we can see from Fig.4 that the first time the defect is observed is 9.12s, and the time for the maximum temperature contrast is 11.4s. This shows that the testing for composite by the thermal wave testing method is better than for metal, because the heat conduction coefficient of composite is smaller than metal, which makes the infrared camera capture more defect information.



Fig.1. The pulsed heating infrared thermal wave non-destructive test system



(a) The steel shell specimen



(b) The composite specimen

Fig.2. Specimens of the experiment

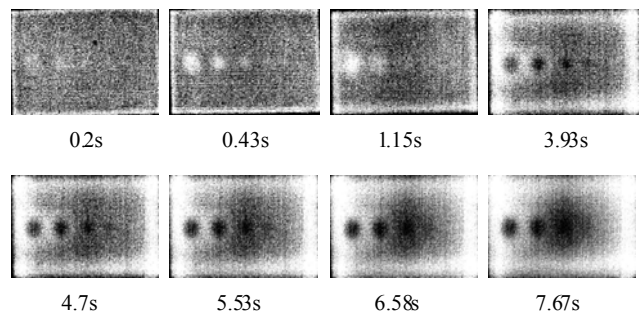


Fig.3. Thermal image sequences of steel shell

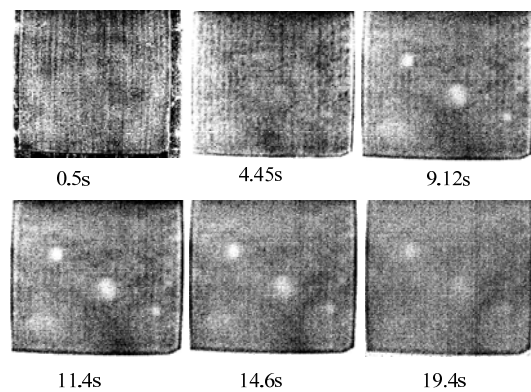
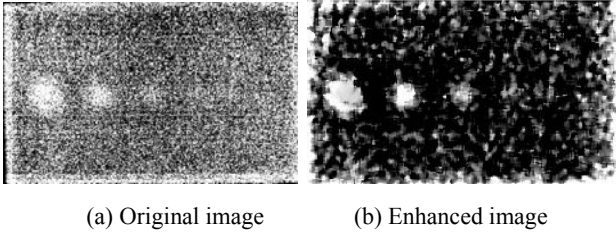


Fig.4. Thermal image sequences of the composite material

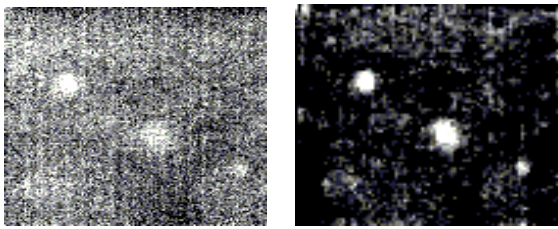
4. IMAGE PROCESSING

The original images are noisy, distorted and their contrast is low. In order to avoid the influence of the noise, the homomorphic filtering technique is used. The enhanced results are shown in Fig.5 and Fig.6.



(a) Original image (b) Enhanced image

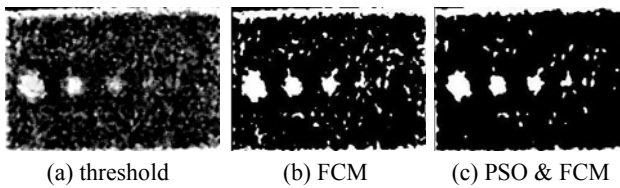
Fig.5. The enhancement image of the steel shell



(a) Original image (b) Enhanced image

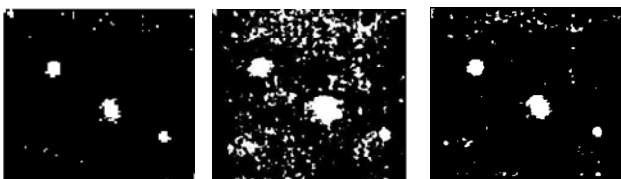
Fig.6. The enhancement image of the composite material

The threshold-based segmentation method, FCM clustering algorithm and the proposed segmentation algorithm are applied to the enhanced thermal images of the steel shell (490 × 285 pixels) and the composite (490 × 460 pixels). In the threshold segmentation, the gray levels the threshold selected were 210 and 180. The parameters of the clustering algorithm based on the PSO were set as:  $c=3$ , the population size  $n=40$ ,  $c_1=c_2=2$ ,  $\omega_{max}=0.9$ ,  $\omega_{min}=0.4$ ,  $m=2$ , the maximum number of iterations 500. The algorithm was implemented in MATLAB7.0. The values of cluster centers were calculated according to the obtained particle swarm algorithm for image segmentation. The results are shown in Fig.7 and Fig.8.



(a) threshold (b) FCM (c) PSO & FCM

Fig7. Segmentation images of the steel shell



(a) threshold (b) FCM (c) PSO & FCM

Fig.8. Segmentation images of the composite material

In order to evaluate the performance of the three algorithms, the correct segmentation rate was introduced, which is defined as [18]:

$$accuracy = \frac{\text{correct pixels}}{\text{all pixels}} \times 100\% \quad (9)$$

The accuracy and the segmentation time of the three segmentation algorithms are shown in Table 1.

5. QUANTITATIVE IDENTIFICATION OF THE DEFECTS

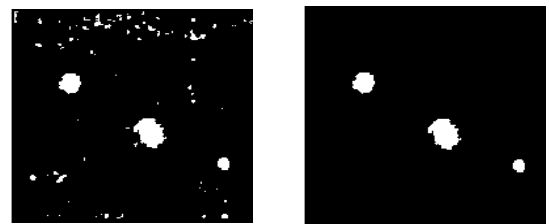
Thermal images obtained in the detection process provided abundant information for analysis of the defects. Every image reflected the temperature field distribution of internal defects. The identification of the defects mainly includes evaluation of their type, depth, size and shape. After the process of enhancement and segmentation, the external noise and interference of the thermal wave images were eliminated. For quantitative evaluation of image segmentation, the quantitative identification of the defects was explored using regional processing. The obtained results are shown in Fig.9.

Table 1. Results of the three algorithms

Algorithm	the segmented images	accuracy	time/s
threshold	the steel shell	77.58%	—
	the composite	87.10%	—
FCM	the steel shell	87.95%	72.1253
	the composite	93.75%	77.4461
PSO & FCM	the steel shell	95.53%	12.8406
	the composite	97.86%	15.7419



(a) The image of the steel shell



(b) The image of the composite

Fig.9. The area disposal results of the segmented images

After the image processing, the defects information can be described as follows:

1. The “imview” function of MATLAB has been used to determine locations of the defects. For the image of steel shell, centers of the defects are (38, 104) (102, 105), (163, 99) and (217, 98). For the composite materials, they are (47, 66), (110, 111) and (164, 136).

2. The defects were extracted separately by the function “bwselect” of MATLAB, and then the areas of the defect (i.e., pixel size, in pixels) have been calculated by the function “bwarea”. For the image of steel shell, the pixel areas are 2411.2429, 1286.1432, 780.9515 and 364.0028. The pixel areas of the composite materials are 1437.3931, 2655.6321 and 522.6321.

3. The calculated area of the defects has been obtained by the proportional relationship (in mm<sup>2</sup>) expressed as:

$$S'_i = \frac{S_{totle}}{P_{totle}} \cdot S_i \quad (10)$$

$$\varepsilon_i = \left| \frac{S'_i - S}{S} \right| \times 100\% \quad (11)$$

where  $S_i$  is the pixel area,  $S_{totle}$  is the total area of the specimen,  $P_{totle}$  is the total pixel number,  $S$  is the theoretical area,  $\varepsilon_i$  is the absolute error. For the steel shell, the thermal image is 490 lines, the column is 285, so the total pixel number  $P_{totle} = 490 \times 285 = 139650$ , and  $S_{totle} = 255 \times 156 = 39780 \text{ mm}^2$ . For composite images, the image is 490 lines, the number of column is 460, so the total pixels  $P_{totle} = 490 \times 460 = 225400$ , and  $S_{totle} = 250 \times 250 = 62500 \text{ mm}^2$ . All the identification results are listed in Table 2 and 3.

From Table 2 and 3, it can be seen that the detection effect for the composite materials is much better than for the steel shell, and the greater the defect, the better the identified result.

Table 2. Positions and superficial characters of the steel shell

Name	Defect 1	Defect 2	Defect 3	Defect 4
Center position	(39.6102, 103.7237)	(102.1269, 103.1750)	(163.4202, 99.4397)	(214.1940, 97.2587)
$S_i$	2411.2429	1205.1432	698.9515	319.0028
$S'_i$	721.1973	343.2850	233.5808	108.8724
$S$	706.86	314.16	176.7	78.54
$\varepsilon_i$	2.03	9.27	12.67	15.70

Table 3. Positions and superficial characters of the composite material specimen

Name	Defect 1	Defect 2	Defect 3)
Center position	(47.2377, 66.0359)	(108.0291, 108.8956)	(164.1975, 136)
$S_i$	1437.3931	2655.6321	522.1025
$S'_i$	398.5673	736.3665	144.7711
$S$	452.39	804.25	153.94
$\varepsilon_i$	11.89	8.44	5.95

## 6. CONCLUSIONS

In order to quantitatively recognize the defects of thermal wave non-destructive detection, the fuzzy C-mean clustering algorithm based on the particle swarm optimization was applied to the thermal image segmentation. The threshold segmentation method and the traditional Fuzzy C-Mean algorithm for image segmentation were applied to contrast

with the algorithm proposed in this paper, using the segmentation accuracy rate. Results show that the speed of the proposed method is five times greater than in the case of the traditional fuzzy C-means algorithm, and the algorithm proposed has the best correct segmentation rate within the three compared methods. The algorithm proposed in this paper is not sensitive to noise or local minimum. It yields accurate image segmentation, and acceptable identification errors. The Fuzzy C-Mean clustering algorithm based on the particle swarm optimization can boost the speed and it can be effectively applied to the thermal wave non-destructive detection for image segmentation.

## ACKNOWLEDGMENTS

We gratefully acknowledge the National Natural Science Foundation of China (No. 51075390, No. 51275518) and Natural Science Basic Research Plan in Shanxi Province of China (No.2012JQ8018) for support for this project.

## REFERENCES

- [1] Liu, B., Zhang, C.L., Feng, L.C. et al. (2007). Edge detection method on thermal wave images for skin-core disbonds in carbon fiber reinforced honeycomb material. *Infrared and Laser Engineering*, 36 (2), 211-213, 273.
- [2] Maldague, X.P.V. (2002). Introduction to NDT by active infrared thermography. *Materials Evaluation*, 6, 1060-1073.
- [3] Yang, X.L., Jiang, T., Feng, L.C. (2009). Thermographic testing for impact damage of airplane composite. *Nondestructive Testing*, 31 (2), 120-122, 143.
- [4] Steven, M.S., Tasdiq, A., Yu, L.H. (2003). Thermographic inspection of composite structures. *SAMPE Journal*, 39 (5), 53-58.
- [5] Takahide, S., Shiro, K. (2002). Applications of pulse heating thermography and lock-in thermography to quantitative nondestructive evaluations. *Infrared Physics & Technology*, 43, 211-218.
- [6] Wang, X., Jin, W.P., Zhang, C.L. (2004). Infrared thermography NDT methods and development. *Nondestructive Testing*, 26 (10), 497-501.
- [7] Barreira, E., de Freitas, V.P. (2007). Evaluation of building materials using infrared thermography. *Construction and Building Materials*, 21, 218-224.
- [8] Marinetti, S., Vavilov, V. (2010). IR thermographic detection and characterization of hidden corrosion in metals. *Corrosion Science*, 52, 865-872.
- [9] Přibil, J., Zařko, B., Frollo, I. et al. (2009). Quantum imaging X-ray CT systems based on GaAs radiation detectors using perspective imaging reconstruction techniques. *Measurement Science Review*, 9 (1), 27-32.
- [10] Mikulka, J., Gescheidtova, E., Bartusek, K. (2012). Soft-tissues image processing: Comparison of traditional segmentation methods with 2D active contour methods. *Measurement Science Review*, 12 (4), 153-161.

- [11] Zhang, X.G., Li, J., Liu, S.Q. (2006). A method of infrared image segment based on mathematical morphology. *Guidance & Fuze*, 12, 40-43.
- [12] Duan, X.D., Wang, C.R., Liu, X.D. (2007). *Particle Swarm Optimization Algorithm and Application*. Shenyang: Press of Liaoning University, 154-184.
- [13] Pakhira, M.K., Bandyopadhyay, S., Maulik, U. (2004). Validity index for crisp and fuzzy cluster. *Pattern Recognition*, 37, 487-501.
- [14] Liu, X.L. (2006). *Research on Fuzzy-Clustering-Based Method of Image Segmentation*. Master dissertation of Hefei University of Technology, Anhui Hefei, China.
- [15] Li, L.L. (2009). *Fuzzy C-Means Algorithm and Its Application in Image Segmentation*. Master dissertation of Shandong Demonstration University, Shandong Jinan, China.
- [16] Yang, Z.W., Zhang, W., Wu, C.Q. et al. (2010). Infrared thermography applied to evaluate adhesive quality of missile motor shell. *Chinese Journal of Scientific Instrument*, 31 (12), 2781-2787.
- [17] Yang, Z.W., Zhang, W., Tian, G. et al. (2011). Infrared thermography applied to detect debond defect in shell structure. *Infrared and Laser Engineering*, 40 (2), 186-191.
- [18] Ahmed, M.N., Yamany, S.M., Mohamed, N. (2002). A modified fuzzy C-means algorithm for bias field estimation and segmentation of MRI data. *IEEE Transactions on Medical Imaging*, 21, 193-195.

Received July 19, 2012.  
Accepted November 20, 2012.